Spring 4-2015

A Microscopic Study on the Corrosion Fatigue of Ultra-Fine Grained and Conventional Al–Mg Alloy

Mala M. Sharma
Bucknell University, msharjud@bucknell.edu

Josh D. Tomedi
Bucknell University

Jeffery M. Parks
Westinghouse Electric Company

Corrosion Science 93 (2015) 180–190

Contents lists available at ScienceDirect

Corrosion Science

journal homepage: www.elsevier.com/locate/corsci

A microscopic study on the corrosion fatigue of ultra-fine grained and conventional Al–Mg alloy

Mala M. Sharma [a,*], Josh D. Tomedi [a], Jeffery M. Parks [b]

[a] Bucknell University, Department of Mechanical Engineering, Lewisburg, PA 17837, USA
[b] Westinghouse Electric Company, Cranberry Township, PA 16066, USA

ARTICLE INFO

Article history:
Received 27 June 2014
Accepted 10 January 2015
Available online 17 January 2015

Keywords:
A. Aluminium
B. SEM
C. Corrosion Fatigue
C. Pitting corrosion

ABSTRACT

The corrosion behavior of a nanocrystalline (NC)/ultrafine grained (UFG) Al–Mg based alloy was investigated and compared to its conventional counterpart 5083(H111). The corrosion fatigue (CF) was studied with respect to pit initiation, pit location and crack propagation as a function of environment. Scanning electron microscopy (SEM) with EDS was used to analyze the fracture surface of the failed specimen with respect to pitting characteristics, crack propagation and corrosion product. Load vs. cycles to failure was measured and *S*/*N* curves were generated for the UFG Al–Mg based alloy and the conventional counterpart 5083 in air and seawater.

1. Introduction

Aluminum alloys are known for being ductile, lightweight and having excellent strength to weight ratios. Unfortunately, the ultimate strength of these alloys is not as high as conventional structural materials like steel. New advances in manufacturing techniques allow precise control over the microstructure evolution which permits tailoring of the microstructure, thus improving the tensile strength and other essential properties such as wear and fatigue. Al 5083 is a predominately aluminum–magnesium based alloy that is often used in marine and naval applications and could benefit from improved strength and fatigue resistance. Reducing the grain size of a material has been shown to improve properties of materials [1,2]. Cryomilling powders to produce nanocrystalline particles and subsequently consolidating into billet form followed by plastic deforming, is one way to produce materials with nanocrystalline (NC) or ultrafine (UFG) grains. UFG and NC materials from Al–Mg alloys have yielded tensile strengths between 520 and 740 MPa which is more than twice the ultimate tensile strength of polycrystalline Al 5083 materials (269–290 MPa) [1,2]. In addition to the high strength, high temperature and increased fatigue properties reported for these fine grained materials, corrosion properties are of particular interest for naval applications [3,4]. The corrosion behavior of fine grained aluminum and magnesium alloys is a significant concern because previous research has shown corrosion resistance to improve and deteriorate based on the processing method, composition, distribution of second phase particles and service environment [2,5–15]. Liao et al. [14] found that fine grained Mg–Al alloys exposed to 0.1 M NaCl solution had superior corrosion resistance when compared to micro-grained hot-extruded alloys of the same composition. They attributed the enhanced corrosion performance to the enhanced passivity of the oxide film that generated on the surface [14]. Similarly, Sharma and Ziemian [2] found the performance of NC/UFG Al 7.5 Mg alloys in atmospheric environment to depend significantly on pitting kinetics which varied based the processing conditions and chemical composition. Understanding the behavior of fine grained materials that will be used in structures, and that are subjected to loading (static and cyclic) while exposed to aggressive environments is of significant importance if they are to be viable for naval applications. The resulting combined action of loading and aggressive environment often results in stress corrosion cracking and corrosion fatigue; both ensuing in damage that significantly reduces a material's fracture resistance. Since reduced fracture resistance can result in serious or catastrophic failure, a study of the environmental degradation mechanisms and fatigue properties of fine grained materials is clearly needed if they are to be used in these applications.

Pitting corrosion is a known damage mechanism affecting the integrity of aluminum materials that are used in structures for naval applications. Most aluminum alloys contain a thin oxide layer on the metal surface which helps to reduce the corrosion rate. However, when localized breakdown of this film occurs, pitting corrosion is the result, thereby promoting accelerated dissolution of the underlying metal. Corrosion pits generally initiate due to a

* Corresponding author. Tel.: +1 570577 1686; fax: +1 5705777281.
E-mail address: mala.sharma@bucknell.edu (M.M. Sharma).

http://dx.doi.org/10.1016/j.corsci.2015.01.020
0010-938X/

chemical or physical heterogeneity at the surface, such as inclusions, second phase particles, flaws, mechanical damage, or dislocations [2–4,16]. The composition of the material, amount, size and distribution of second phase particles and type of electrolyte will all have an effect on the corrosive mechanisms that result [17–19]. Burstein et al. [20] studied the origins of pitting corrosion, and revealed that pit nucleation occurs at the microscopic level with some metals displaying preferential sites for pit nucleation. Naval alloys contain various constituent particles for strengthening which play a significant role in corrosion pit formation [17–19]. Many studies have utilized optical microscopy, scanning electron microscopy (SEM), transmission electron microscopy (TEM) and atomic force microscopy (AFM) techniques to better understand particle-induced pitting corrosion in aluminum alloys [2,16,21]. For the most part, corrosion fatigue initiates with pitting and subsequent crack formation, and ends with the propagation of the crack initiated at the base of the pits. As a result, it can be said that pitting directly activates crack initiation earlier [16–19] and can significantly affect the fatigue life of aluminum alloys used in naval applications.

The resistance to fatigue crack initiation and propagation of metals and alloys is also known to be influenced significantly by grain size [22]. Based on the Hall–Petch relationship, and the basis of experimental results obtained in conventional microcrystalline metals, it is widely accepted that an increase in grain size generally results in a reduction in the fatigue endurance limit. However, for nanocrystalline materials, this law to a certain extent is not observed, giving way to the so-called inverse Hall–Petch effect; which is a mechanism currently not well understood. Such lack of understanding is primarily a consequence of the lack of experimental data on the fatigue response of metals with very fine grains. Tensile properties and fatigue crack growth have been investigated for ultrafine grained (UFG) and nanocrystalline Al–Mg alloys [23–25]. However, a direct comparison of the cause of fatigue crack initiation, propagation and behavior in marine environments of the very small grain size Al–Mg alloy to larger grain sized materials of similar composition has not been made. Therefore, the objective of this study is to investigate the corrosion fatigue behavior of an UFG Al–Mg alloy and compare the results to a conventionally processed micrograined alloy of similar composition.

2. Experimental procedure

Two aluminum alloys were used to study the effects of a finer grain size and manufacturing method on the corrosion fatigue behavior of the aluminum–magnesium alloys. The materials chosen were a conventionally processed 5083-H111 Al–Mg alloy and an ultra fine grained (UFG) partially nanocrystalline (NC) Al–7.5 Mg alloy. The aluminum alloy 5083-H111 can be classified as a wrought alloy product. Al 5083-H111 was chosen because of its common marine applications and excellent corrosion resistance. Currently, the Navy uses Al 5083 for all topside marine atmospheric exposure conditions. The H111 temper was chosen based on the similarity to the manufacturing process of the UFG alloy. The compositions of the Al 5083-H111 and UGF Al–Mg alloys, in weight percent, are given in Table 1.

Table 1
Composition of Al–Mg alloys investigated.

Element	Alloy compositions in weight percent	
	5083-H111	UFG Al–7.5 Mg
Mg	4.90	7.50
Fe	0.31	0.09
Cr	0.13	–
Mn	0.40	–

2.1. Material processing

The UFG Al–7.5 Mg alloy was manufactured by the Boeing Company in collaboration with the University of California, Irvine. The material was processed through a combination of cryomilling and hot isostatic pressing. Spray atomized powders, with an average particle size less than 150 μm, were mechanically milled in liquid nitrogen through cryomilling to reduce the grain size. After cryomilling, the powder had a grain size of approximately 30 nm. The powder was then heated to 300 °C under a vacuum of 10^{-6} Torr for degassing. Powder was consolidated by hot isostatic pressing (HIP) at 250 °C under a pressure of 200 MPa. Finally, the material was extruded at an extrusion ratio of 20:1 for the UFG Al–7.5 Mg. In order to help interpret the data obtained in this study, reference is made to previous work investigating the localized corrosion and pitting behavior of these same alloys [2,26].

2.2. Specimen design

The shape and dimensions of test samples are shown in Fig. 1. The samples used in fatigue testing were smooth round dog-bone specimens, machined in the longitudinal direction, where the loading axis paralleled the extrusion direction. To investigate the fatigue behavior of the alloys, a smooth groove was machined into the samples to reduce the smooth gauge section and thus increase the foregoing area ratio. Effectively, the diameter of the specimen was reduced from the original 3.81 mm to nominally 1.6 mm at the notch. The notch radius was 6.35 mm. This was done to execute a timely test and because pre-tests without the smooth groove indicated the samples to be notch sensitive when they failed in the threaded grip section. Replicate samples were prepared from the same extrusion for each respective material. Round bars were first wire EDM'd (Electro-Discharge Machined) from the extrusion and then machined to the final dimensions. The surface finish of the material in the gauge section was polished to 1200 grit.

2.3. Fatigue testing

Uniaxial tension–tension fatigue tests were conducted at the LaQue Center for Corrosion Technology (LCCT) in Wrightsville Beach, North Carolina. The tests were executed at a stress ratio R (min/max) of 0.1 using a sinusoidal cyclic frequency of 20 Hz in air and 1 Hz in natural seawater. To generate S–N curves in air and seawater for the UFG Al–7.5 Mg alloy, fatigue specimens were loaded to various maximum stress levels between 173 and 420 MPa and the cycles to failure noted. For the conventional 5083 alloy, maximum stress levels between 173 and 310 MPa were used. Preliminary testing helped identify the best range of maximum stress values to use for each respective alloy. To test

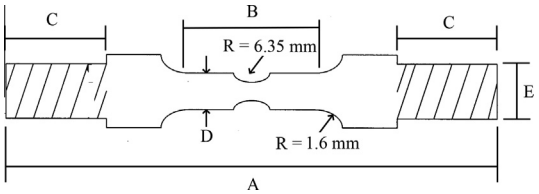

Fig. 1. Shape and dimensions of test specimen: smooth round tensile bar specimen with a round groove machined in the gauge section for corrosion fatigue testing. The dimensions are as follows: A = 50 mm, B = 12.7 mm, C = 3.8 mm, D = 12.7, E = 6.35 mm.

the specimen, an MTS 810 servo hydraulic system was employed using Model 490 digital controller and Test Star software.

2.4. SEM/EDS analysis of fatigue specimens

In order to form any conclusions concerning the effects of pitting on the fatigue life of a material, it is necessary to evaluate the cause and location of fatigue crack initiation, as well as the propagation of the fatigue crack until ultimate failure occurs. For this reason all fracture surfaces were evaluated. This included the characterization of failure initiation and failure mechanisms such as inclusions, material defects and corrosive pitting products based on the location of the crack (internal, external at a pit), as well as studying the propagation of the fatigue crack for all specimens.

Fatigue crack propagation up to failure was estimated through the calculation of the approximate area of crack advancement in the propagation zone before the fracture zone. Measurements consisted of the maximum crack depth, and the width of the crack area at the surface. These values were then entered into a Matlab program, to estimate the total area loss due to fatigue crack growth before failure. Characteristics were then related to fatigue data for each specimen to determine if there was a correlation between crack growth, pitting and fatigue life for nanostructured specimens subjected to a marine environment.

3. Results and discussion

3.1. Conventional 5083-air

The results for the conventional 5083 H111 alloy are presented in Fig. 2. The *S–N* curves show that for the conventional 5083 H111 alloy, cycles to failure in seawater match fairly well with those conducted in air for a wide range of maximum stress values, Fig. 2a. This trend begins to change around 275 MPa and significantly changes around maximum stress values of 207 MPa or less, where cycles to failure are greater than 1×10^6 (Fig. 2b). At this point, the cycles to failure vary by a factor of 1 between seawater and air. This may indicate that for the conventional 5083 alloy, under cyclic loading in a natural seawater environment at low maximum stress values, pits do not initiate until after many high cycles to failure. It may also mean that pits do not have as significant effect at higher maximum stress levels, but at lower values there is time for the corrosion mechanism to grow and dominate failure. Another possibility is that a crack closure mechanism is at work at higher stress levels due to build-up of corrosion product, which blunts the crack. To help elucidate this behavior the fracture surfaces were examined closely.

The macroscopic fracture morphology of the fatigue samples in air were similar to those which fractured under uniaxial tensile loading and slow strain rate testing [2,15]; the specimen fractured with very little shear lip on the periphery of the sample, and the fracture surface was normal to the axial loading direction. Additionally, it was noted that irrespective of applied maximum stress, failure occurred when a crack initiated at an inside inclusion near the specimen surface, Fig. 3. It is possible that this type of crack was initiated by interfacial debonding between the matrix and inclusion due to stress concentration, and/or by fracture of the inclusion itself. EDS elemental analysis showed that the inclusions were comprised of various amounts of Al (Fe, Cr, Mn), and are cathodic particles relative to the matrix over which the oxygen reduction reaction takes place [24]. SEM with EDS also identified evidence of Al, Mg, Si and Bi oxide inclusions

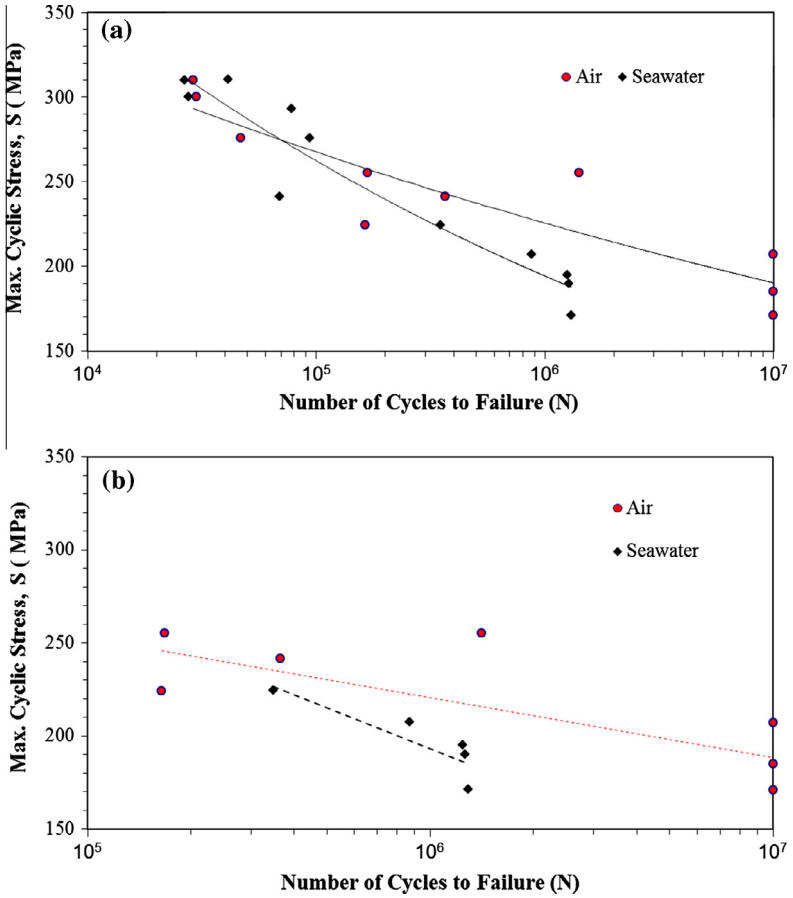

Fig. 2. *S–N* curves for the fatigue performance of conventional 5083-H111 in air and seawater (a) for cycles 1.9×10^4–1.9×10^6 (b) for cycles 1.0×10^5–1.0×10^7.

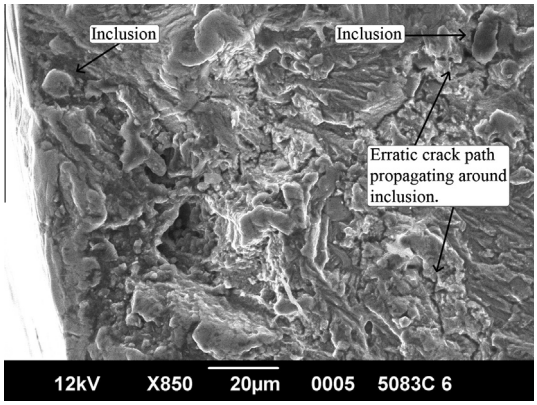

Fig. 3. SEM micrograph of the fracture surface of conventional 5083 showing crack initiation at various second phase inclusions and crack pattern.

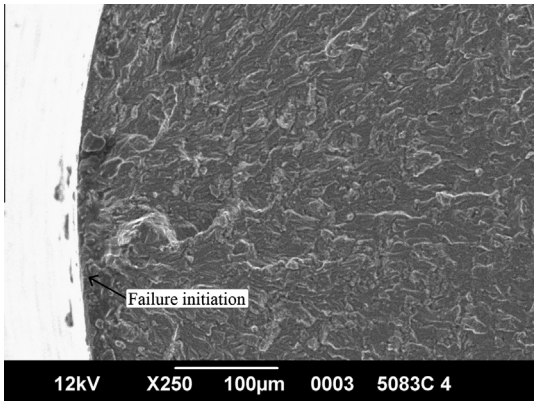

Fig. 4. SEM micrograph of the fracture surface near the crack initiation site on a conventional 5083 alloy. The fracture surface is transgranular, and macroscopically appears relatively flat.

which are inherent problems in powder metallurgy manufacturing methods. Table 2 shows the tabulated chemical compositions of the inclusions. These results indicate that the amount of inclusions (size and distribution) in the material should be decreased to improve fatigue strength of the conventional 5083 alloy. SEM examination of the fracture surface near the crack initiation site revealed the fracture surface was transgranular, and macroscopically appeared relatively flat due to the fact that the grain size of the material is somewhat small (Fig. 4). Following the fatigue crack as it extends, intergranular cracking can be observed in addition to the transgranular cracking. Just before final catastrophic failure, ductile dimples as well as the fracture of intermetallic second phase particle are also observed, Fig. 5. The crack path for the conventional 5083 was erratic and resembled somewhat of a zig zag pattern as the crack propagated around second phase inclusions (Fig. 3).

3.2. Conventional 5083–3.5% NaCl

A number of theories exist to describe the mechanisms of environmental degradation and crack propagation in Al–Mg alloys; the three most prominent are based on (1) film rupture related to IGSCC, (2) propagation via corrosion tunneling and (3) environmental crack propagation driven by hydrogen embrittlement. Material characteristics such as stability of the passive film and repassivation kinetics play a significant role in the behavior as well as anodic dissolution kinetics at the sensitized grain boundaries and material properties such as ductility, toughness and yield strength. Anodic dissolution of the β-phase is prominent in all three previously stated mechanisms. Passivation behavior is related to film rupture and hydrogen embrittlement while corrosion tunneling is controlled mostly by material properties. Electrochemical behavior at the crack tip and the interactions of the crack tip with the microstructure of the material will ultimately control the mechanisms of environmental degradation.

Table 2
EDX analysis of inclusions with chemical compositions in weight percent.

Inclusion	Mg	Al	Mn	Fe	Cr	Si	Bi	O
1		63.71	11.24	4.78	0.02	–	–	–
2	–	56.21	4.91	13.42	0.01	–	–	–
3	63.35	2.12	–	–	–	34.53	–	–
4	–	71.32	–	–	–	–	6.44	22.24
5	–	77.73	3.42	2.73	2.94	3.12	–	–
Al-rich matrix	4.67	95.24	–	–	–	.09		–

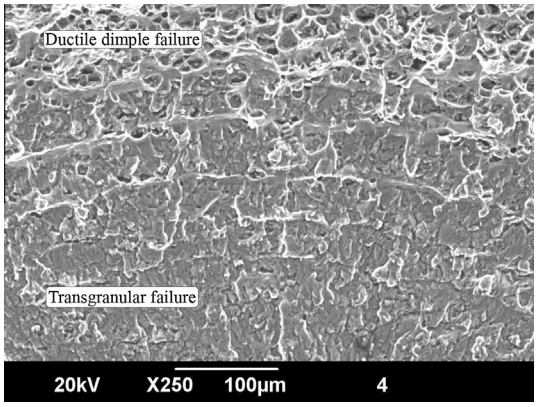

Fig. 5. SEM micrograph of the fracture surface for conventional 5083 alloy showing evidence of both transgranular and ductile dimple rupture.

Microscopic investigation of the conventional 5083 fatigue samples tested in 3.5% NaCl revealed that a crack that caused final failure in the corrosion fatigue samples was typically initiated at either an inclusion, or corrosion pit which formed around the inclusion, Fig. 6. The Al (Fe, Cr, Mn) precipitates detected by EDS are known to be affected by localized alkaline corrosion (LAC). The process occurs as a result of the alkalization of material surrounding the cathodic particles in the matrix [27,28]. The morphology of the pits which result from this process is considered to be

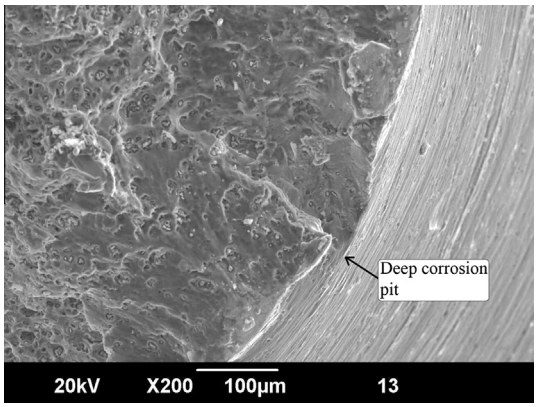

Fig. 6. SEM micrograph showing a deep corrosion pit which formed on the external surface of the conventional 5083 alloy in the marine environment.

irregular and diverts from crystallographic pitting. In this study, when the corrosion fatigue life was extremely short (i.e. 242 MPa) a large inclusion defect was at the location of the initiation site, Fig. 7. This large decrease in fatigue life compared to the other samples is believed to be a direct result of the large inclusion which created a stress concentration, cracking and then pitting. Evidence of dissolution of anodic β-phase particles promoting crack initiation resulting in the decrease in corrosion fatigue life of the conventional 5083 alloy was also observed. The β phase precipitate does not significantly enhance the strengthening properties [29], but instead makes the alloy more susceptible to intergranular and stress corrosion cracking [30]. Literature has reported that the β-phase (Al_3Mg_2) is anodic to the Al-matrix [15,31]. Due to the fact this phase is anodic its presence enhances the selective dissolution at grain boundaries thus creating sites for deep pits to form when under static tensile fatigue loads. In this study, the corrosion pits tended to form perpendicular to the extrusion direction. Under the fatigue loading in a corrosive environment, these pits grew and coalesced, resulting in significant crack propagation and growth from the initiation site. This behavior has been noted in previous work on the same alloys [2,15,26]. In a few cases, a large corrosion defect was formed around an inclusion inside the specimen near the external surface (Fig. 8). This would further decrease the corrosion fatigue strength of the material. It is possible that such large corrosion defects occurred due to the localized segregation of constituent materials. Aballe et al. [28] believed that surface finish affected the LAC as much as, if not more than, the variation in number of intermetallic particles. They found that surface density of cathodic particles was a factor of the surface finish grit and resulting surface rugosity; and lower grit surface finish resulted in a lower observed density of particles. Based on these results, in this study, the fine surface finish of 1200 grit would result in a higher density of cathodic intermetallic particles exposed at the surface, a lower surface rugosity and a higher susceptibility to localized corrosion. Similar results have been noted in other aluminum alloys such as AA 6061 and AA 7075 [32–35]. When large second phase inclusions were not present it appears the corrosion fatigue performance was determined by slip enhanced (anodic) dissolution around constituent particles as evidenced in the microstructure at high magnification (Fig. 9) where intermetallic phases, such as Al_3Mg_2 [26], Al_3Mg_5 and Mg_2Si, are anodic with respect to the 5083 alloy matrix and promote rapid localized attack through galvanic interaction. Cathodic corrosion was also a significant factor in the fatigue performance of the conventional 5083 alloys as large pits formed around the particles that are cathodic to the matrix.

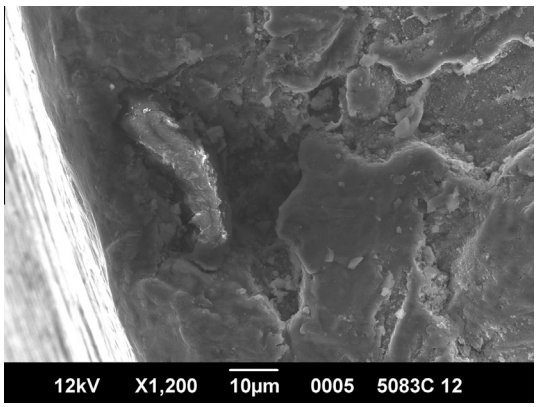

Fig. 8. SEM micrograph of conventional 5083 alloy tested in marine environment showing a large pit which formed around a cathodic particle and creating the crack initiation point.

Despite the extensive amount of studies done on Mg [13,14,36–40] and Al-based [2,15,23–31] alloys, there is not enough clarity regarding the role that the intermetallic particles play in the corrosion behavior. Small-scale particles such as Al_3Mg_2 (Mg_2Al_3) and $Mg_{17}Al_{12}$ affect the pitting behavior and thus subsequent corrosion performance of Al and Mg-based alloys; these intermetallics can be found on the Al–Mg binary phase diagram. In salt solutions similar to natural seawater (3–3.5% NaCl) both these second phase particles have lower corrosion rates than pure or alloyed magnesium, but not pure aluminum [41,42]. Literature has reported that Al_3Mg_2, is more active than pure aluminum and will corrode preferentially with potentials being less noble than most aluminum alloys [31,43,44]. The alloys in this study have enough magnesium to contribute to super saturation of the element and leads to solid solution strengthening at temperatures below ~200 °C. However, this concentration also yields an abundance of the β-phase (Mg_2Al_3) which is known to be deleterious to the corrosion performance [45–48]. The formation of the β-phase is associated with susceptibility to intergranular corrosion (IGC), localized corrosion, stress corrosion cracking (SCC) as well as corrosion fatigue (CF); with the worst case scenarios if the phase is located at the grain boundaries [49–52]. Although there has not been a complete evaluation of the electrochemical behavior of the β-phase in aluminum–magnesium alloys, some researchers have explained the polarization of this phase by the anodic behavior of Al and cathodic behavior of Mg [53–55]. Other researchers [56–62] found dealloying of Mg to play a significant role in the corrosion fatigue and stress corrosion

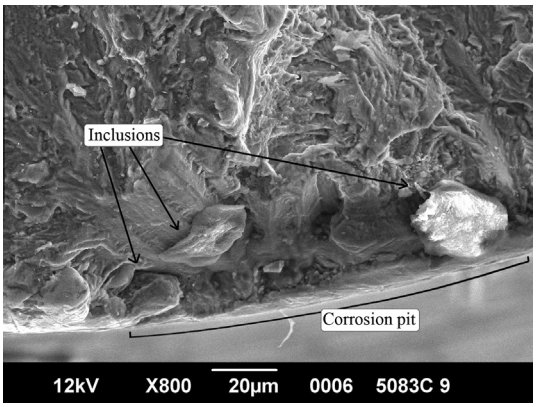

Fig. 7. SEM micrograph of fracture surface of conventional 5083 alloy after fatigue testing showing where failure initiated at several second phase inclusions by creating a large corrosion pit.

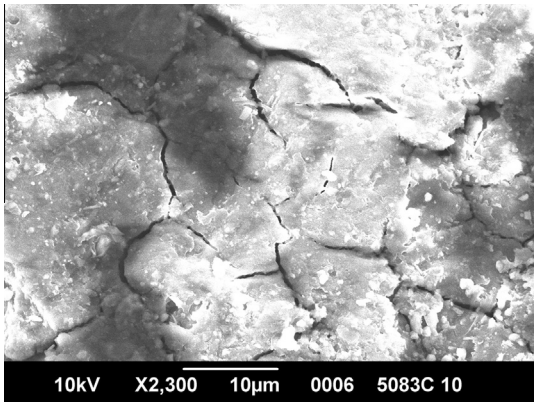

Fig. 9. High magnification SEM micrograph of the failed surface of conventional 5083 alloy after corrosion fatigue showing evidence of anodic dissolution.

cracking of Al–Mg alloys because it produces in an extremely brittle surface layer which can lead to failure. Liu et al. [63] and Yasakau et al. [64] specifically observed Mg dealloying in Al_3Mg_2 and Mg_2Si intermetallics after immersing AA5083 alloys in NaCl solutions. Other researchers have observed Mg dealloying in Al-alloys, Cu–Al alloys and metallic glasses [65,66]. Dealloying is known to be dependent on the electrochemical potential where a porous structure will result under the conditions when the potential range is above the dissolution potential of the more active element while concurrently being below the dissolution potential of the noble element. Dissolution of both elements and subsequent deposition of the more noble element occurs at highly positive potentials [56].

The crack growth morphology of conventional 5083 in both environments exhibited signs of transgranular progression over a much rougher and more tortuous fracture surface, then, an inter/transgranular region followed by ductile dimple rupture.

3.3. UGF Al–7.5 Mg

The *S–N* curves of the UFG Al–7.5 Mg alloy in air and natural seawater are presented in Fig. 10. At higher applied maximum stress, the fatigue performance in natural seawater compared well with that in air. This trend breaks down lower applied maximum stress values around 276 MPa where the fatigue performance varies by a factor of up to 2 (with respect to the number of cycles) (Fig. 10a). This performance shows that the natural seawater environment has a significant effect on the corrosion fatigue resistance of the UFG Al–7.5 Mg alloy. The reason for this decrease in resistance is believed to be attributed to the microstructural features as well as grain size difference.

There appears to be two distinct linear logarithmic trends representing the UFG Al–7.5 Mg corrosion fatigue specimen failures. Fig. 10b shows two trends that represent the upper and lower cyclic fatigue threshold. Specimens representing the lower fatigue trend all showed signs of crack initiation at tiny anodic pits, suggesting that pitting plays a role in the premature failure of nanostructured specimens. Cyclic failure patterns suggest that pitting could substantially inhibit the fatigue life over a maximum cyclic stress range from 207 MPa to 290 MPa, resulting in a decrease in fatigue life of between 57% and 67%. Fig. 11 shows the fracture surface of a sample tested at 207 MPa max stress where multiple tiny pits led to multiple crack initiation sites and ultimate failure. This behavior is indicative of the tunneling effect which has been explained by using the fundamental assumption that extremely thin corrosion tunnels form in a periodic arrangement as a result of anodic dissolution of the β-phase. The tunnels will grow until the ligament can no longer withstand the stress, the material will deform ductility and then ultimately fracture [67]. Pitting appears to have less influence at maximum stresses above this range, where failure was predominately initiated at second phase cathodic inclusions as well as tiny pits which acted as stress concentrators initiating mechanical failure (Fig. 12).

In order to see the effects of grain size variation on the alloys, *S–N* curves for both UFG Al–7.5 Mg and conventional 5083 alloy were compared in air and seawater. Fig. 13 shows the maximum stress vs. the cycles to failure for both alloys in laboratory air. At a maximum stress of 276 MPa, the UFG Al–Mg alloy performs a margin of over 2 fold cycles more than the conventional 5083 alloy. The conventional 5083 alloy reaches run out (10 million cycles), before failure, at a maximum stress of 173 MPa, however, the UFG Al–7.5 Mg alloy reaches run out at much higher maximum stress of ~310 MPa. Although the processing conditions for these two alloys are different, it is evident from Fig. 13 that a reduction in grain size from micro-grained to ultra-fine or nano grained material can improve fatigue performance. It can be said that the high cycle fatigue strength of the UFG Al–7.5 Mg alloy is superior to that of the conventional 5083 alloy in an air environment. Similar results were obtained by Hanlon et al. [68], who investigated fatigue crack growth rate on the fatigue response of electrodeposited nanocrystalline pure Ni and a cryomilled ultra-fine-crystalline Al–Mg alloy. They found that grain refinement generally leads to an increase in the resistance to failure under stress controlled fatigue environment. Conversely, they also observed that with a change in grain refinement from micro- to ultra fine-grained material, a deleterious effect was seen on the resistance to fatigue crack growth. There was a noticeable reduction in ΔK_{th} and a significant increase in the rate of fatigue crack growth from threshold to final failure. The stress intensity factor range for catastrophic failure, which is representative of the fracture toughness and static-mode failure mechanisms, for the ultra-fine crystalline Al–7.5 Mg alloy was also noted to be several times smaller than that for the conventional

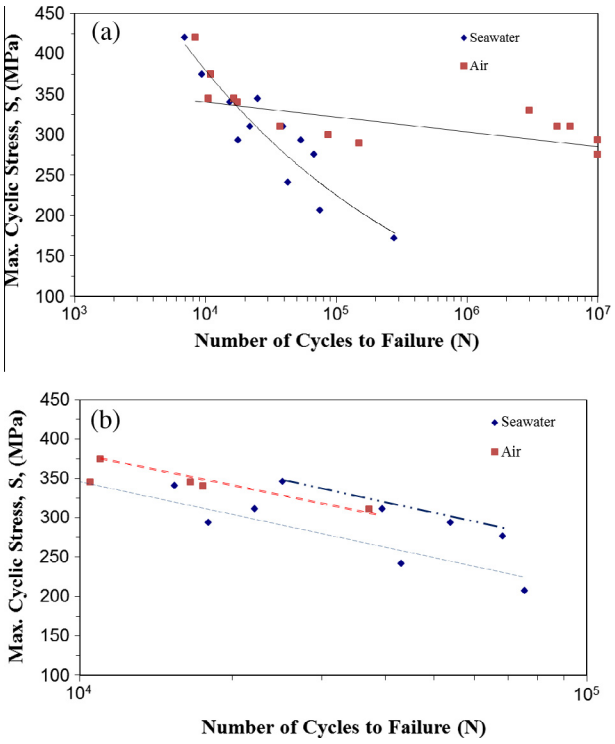

Fig. 10. *S–N* curves for the fatigue performance of UFG Al–7.5 Mg in air and seawater (a) for cycles 1.0 E + 03–1.0 E + 07 (b) for cycles 1.0 E + 04–1.0 E + 05.

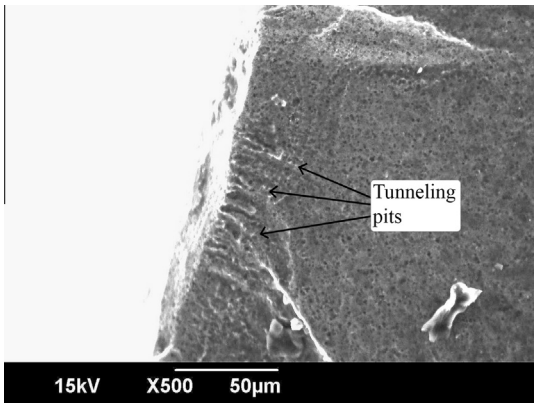

Fig. 11. SEM micrograph showing the fracture surface of UFG Al–7.5 Mg alloy tested in marine environment. Tiny deep pits that had a tunneling effect can be seen.

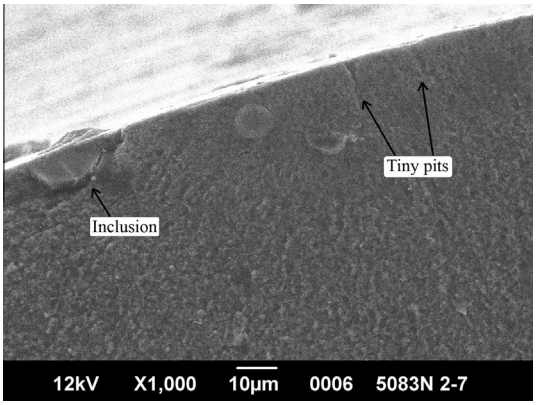

Fig. 12. SEM micrograph showing the fracture surface of UFG Al–7.5 Mg alloy tested in marine environment. Failure at a large second phase inclusion located near the external surface can be observed along with a few tiny anodic pits.

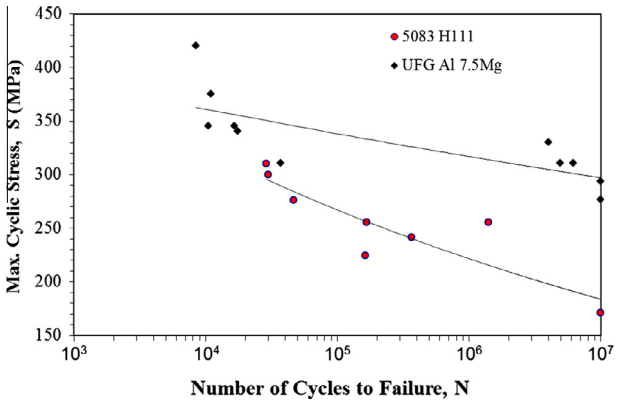

Fig. 13. Fatigue behavior comparing the performance of 5083 H111 and UFG Al–7.5 Mg in air.

5083 aluminum alloy [68]. Pao et al. [69] confirmed these observation in their study of cryomilled UFG Al–7.5 Mg. They attributed the higher fatigue crack growth rates and lower thresholds to the much smoother fracture surface morphology and lower roughness induced crack closure in bulk UFG Al–7.5 Mg. They observed the fatigue crack growth thresholds in air exhibited only a weak stress ratio dependency and identified them as having a Class I behavior when using the fatigue classification proposed by Sadananda and Vasudevan [70]. From their work, Pao et al. [69] concluded that at intermediate and high stress intensities, fatigue crack growth rates of bulk UFG Al–7.5 Mg in 3.5% NaCl solution are higher than those obtained in air.

Fig. 14 shows the generated *S–N* curves for both the alloys in a natural seawater environment. The superior corrosion fatigue resistance of the UFG alloy compared to the conventional 5083 alloy breaks down around an applied max stress of 275 MPa. Anywhere above this stress range, the UFG Al–7.5 Mg alloy compares well, and above 300 MPa even surpasses the conventional 5083 at high maximum stress values.

Since the alloys exhibit different fatigue behavior in an inert environment (dry air), the real extent of corrosion fatigue susceptibility should be examined by comparing the results in an aqueous environment to the fatigue results in dry air. In order to elucidate this, the relative fatigue strength ($\Delta\sigma_{NaCl}/\Delta\sigma_{air}$) vs. cycles to failure for both materials was plotted. A smaller fatigue strength ratio means a higher degree of corrosion fatigue susceptibility for the material based on a specific number of cycles to failure. The diagram in Fig. 15 indicates that the UFG Al–7.5 Mg alloy is more

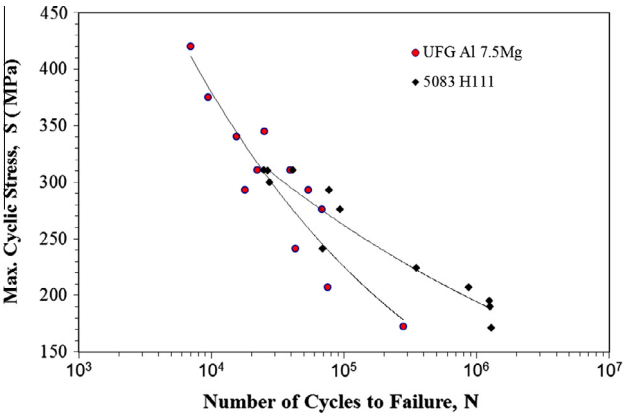

Fig. 14. Fatigue performance comparison of 5083 H111 and UFG Al–7.5 Mg in natural seawater.

susceptible to corrosion fatigue than the conventional 5083 H111 alloy. This difference in susceptibility between the conventional and UFG Al–7.5 Mg alloy increases significantly as the fatigue life increased (*i.e.* as the maximum applied cyclic stress was reduced).

In an aqueous environment, corrosion fatigue crack initiation which is associated with anodic dissolution can be attributed to up to three mechanisms [71–74]. These are: (1) pits that form and cause a stress concentration at the bottom of the formation (2) breakdown of the protective passive film on the metal with an associated chemical attack in the same location and (3) electrochemical attack to plastically deformed areas of a metal where the undeformed areas act as a large cathode. Evidence from the scanning electron microscopy analysis of the UFG Al 7.5 Mg shows that the corrosion fatigue resistance of these alloys is determined by both slip enhanced (anodic) dissolution and hydrogen embrittlement at high stress ranges, while at low stress ranges, the corrosion life is predominately controlled by pitting induced crack initiation. Fig. 16 shows a pit, approximately 30 μm deep which formed on the external surface of the UFG Al–7.5 Mg alloy and led to crack initiation and failure; intergranular fallout and the contour inside of the pit can be observed (Fig. 17). Fig. 18 shows the anodic dissolution and hydrogen embrittlement which also occurred and lead to fatigue crack initiation. In addition to anodic dissolution, hydrogen embrittlement is a governing mechanism that can be used to describe the accelerated crack growth in the

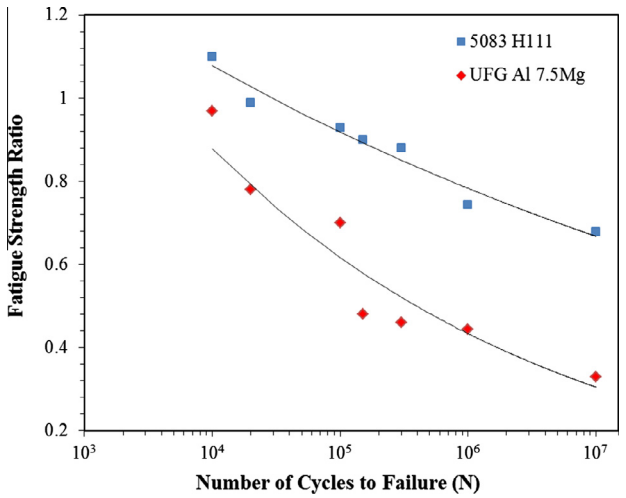

Fig. 15. Relative fatigue strength of 5083 H111 and UFG Al–7.5 Mg alloys as a function of number of cycles to failure.

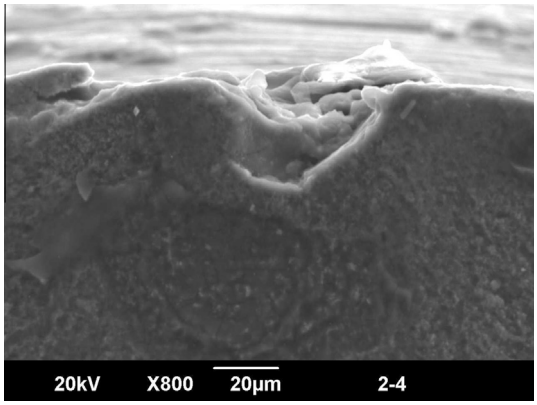

Fig. 16. SEM micrograph of failed corrosion fatigue sample for UFG Al–7.5 Mg alloy tested in the marine environment. A large corrosion pit approximately 30 µm deep formed at the surface of the specimen. Intergranular fall out can be observed inside the pit.

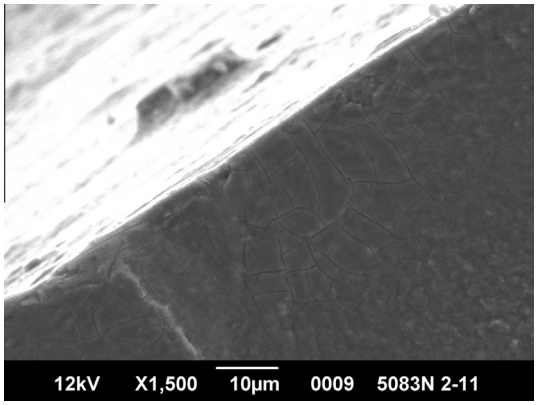

Fig. 18. SEM micrograph of failed surface of UFG Al–7.5 Mg alloy showing anodic dissolution and hydrogen embrittlement which led to failure initiation.

UFG alloys. Menzemer and Srivatsan [75] found hydrogen embrittlement to be the fundamental reason for accelerated crack growth in AA5456 alloys. Jones et al. [76,77] have described the process of hydrogen embrittlement for AA 5083 alloys through a series of detailed steps: (1) mechanical interaction between the crack and β-phase particle whereby the crack may get trapped, (2) preferential corrosion of the β-phase which converts the particle to Al_2O_3, (3) hydrogen evolution occurs as a result of corrosion of the β-phase which then absorbed and diffuses ahead of crack, (4) subsequent crack propagation through or around the particle with concurrent hydrogen uptake, (5) the crack will advance towards the next particle by the hydrogen induced process, whereby it will be eventually halted by mechanical interaction, (6) the process starts all over again. During the process of fatigue in a corrosive environment, hydrogen embrittlement accelerates crack growth by the buildup of hydrogen pressure in the internal voids ahead of the crack tip, thus increasing crack tip stress intensity. Jones et al. [77] described possible crack-tip/particle interactions for electrochemically active particles by discussing the anodic and cathodic particles separately. Those anodic to the matrix will cathodically protect the matrix. The particle dissolution occurs prior to the advancement of the crack and the cracks advance between particles by hydrogen induced growth or dissolution. When examining the effect of particles cathodic to the matrix, Jones et al. [77] found the matrix will cathodically protect the particle. In this situation, crack propagation occurs by particle/matrix interface dissolution along with concomitant mechanical fracture. This fracture can be of the particle matrix interface or the particle itself; this can occur with or without hydrogen. Similar to the mechanisms of stress corrosion cracking, the manifestation of hydrogen concentrated at the crack tip will lead to highly localized stresses. These stresses will subsequently result in failure, once the critical strain is reached. In corrosion fatigue the surface oxide layer is continually fractured due to the cycle nature of the loading. This process consistently exposes a new surface which reacts with constituents in the environment, thus creating a more intense crack growth [75,78].

The fracture surface exposing the crack growth morphology of UFG Al–7.5 Mg is smooth, flat and generally uncharacteristic in the initial fast crack propagation zone. Due to the fine grain size of the material, it was very difficult to tell if the crack path was intergranular, transgranular or a combination of both. A separate study, however, observed transgranular crack paths in UFG Al–7.5 Mg materials [68]. Striations were noted without any significant observations of ductile dimple rupture before ultimate failure (Fig. 19). The crack pattern is relatively straight initially before hitting the striations, Fig. 20. The main difference in fracture surface between the two environments was that samples in seawater displayed multiple crack initiation sites (greater than three) whereas those in air usually displayed only one or two.

Similar fracture morphologies and locations of failure initiation have also been reported for other nanostructured and UFG materials [79–81]. Near surface internal defects are sites for fatigue crack initiation in both UFG and conventional microcrystalline alloys and

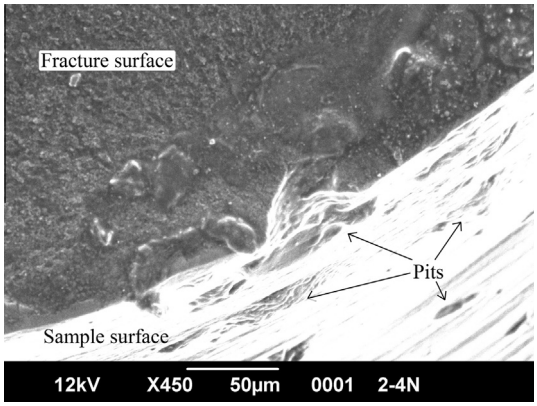

Fig. 17. SEM micrograph of failed corrosion fatigue sample for UFG Al–7.5 Mg alloy the contour inside the pit can be observed.

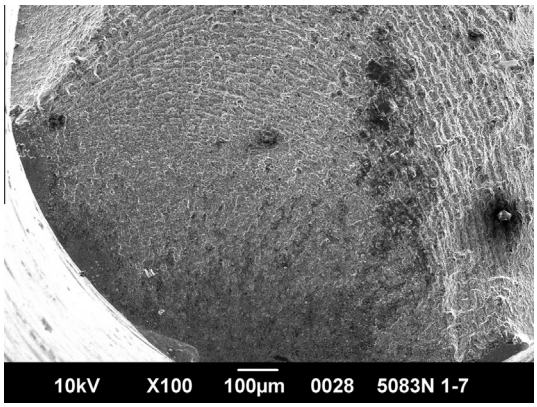

Fig. 19. SEM micrograph showing failed surface of UFG Al–7.5 Mg alloy after fatigue testing in air. Striations can be seen but no significant evidence of ductile dimple rupture before ultimate failure can be observed.

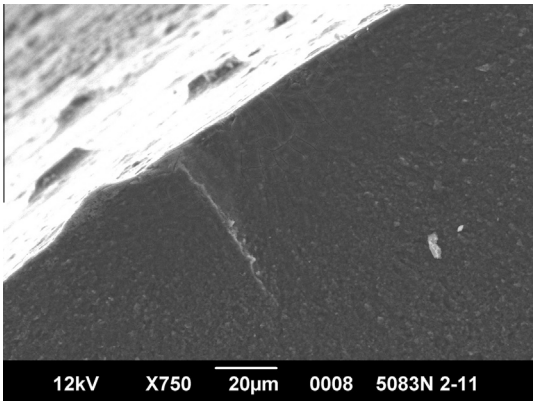

Fig. 20. SEM micrograph showing failed UFG Al–7.5 Mg alloy tested in marine environment with a very straight crack path.

when minimized, failure usually occurs at the surface of the specimen. Boyce et al. [81] found surface oxides from the manufacturing processes to be particularly harmful to fatigue performance. Fatigue crack growth experiments by Yang et al. [80] on NC LIGA Ni identified various different fracture surfaces which correspond to different regimes of crack growth. Observations included flat crack growth in the near-threshold regime, fatigue striations in the Paris regime, striation with an accompanied dimpled region in the high ΔK regime, and ductile dimpled rupture in the overload failure regime. The authors attributed the specific characteristic of crack growth to the microstructure of the materials, a reduction in grain size and the associated limited ductility [80].

From a related study [2] it was found that the sharp geometric shape of pits on the surface of the conventional alloy tested in chloride solutions were irregularly shaped and clustered in various areas throughout the specimen while the UFG Al–7.5 Mg alloy had smoother, more equiaxed shaped pits that were more evenly distributed. The greatest variation between the two alloys occurred in the pit size, distribution and depth [2]. The conventional Al 5083 alloy had more significant damage due to pitting as far as quantity and size of pits but it was observed that the pit depth for the conventional material was only half that observed for the UFG Al–7.5 Mg alloy and was a result of the intergranular corrosion susceptibility of the UFG alloys [2,26]. More specifically, it was observed that the grain boundaries of the nano Al–7.5 Mg alloy was seriously corroded with many grains having fallen out while the grain boundaries of the conventional 5083 were left intact. Additionally, the corrosion attack was observed only around precipitates, not grain boundaries for the conventional alloy [26].

In the overall fatigue life of a material the fraction of the cycles required for fatigue initiation and failure varies. This behavior shows a strong dependence on both the microstructure of the material and the environment. Under cyclic loading, the corrosion fatigue strength of both alloys became lower than that conducted in air, because pitting corrosion on the sample surface acted as a stress concentrator. Crack initiation sites resulting in fatigue failure were at inclusions or second phase particles. The difference in corrosion fatigue susceptibility between the two alloys is believed to be based on the location, size, number and type of pits that were formed. This shows a need for processing materials with finer; more evenly distributed second phase particles.

3.4. Analysis of fatigue crack propagation

The estimated area loss due to fatigue crack propagation before failure for the UFG samples ranged from 10.64% to 30.67%; while the estimated area loss for conventional specimens ranged from 3.22% to 25.31%. This behavior did not change based on environment; ranges for crack profiles were similar whether specimen were tested in air or seawater for respective materials. Additionally, no correlation was found between estimated size of area loss and the maximum applied fatigue load. The main deduction was that the range of estimated area loss for the UFG Al 7.5 Mg alloys was significantly higher than that of the conventional 5083 H111 alloys. This information may be used to support the idea that crack propagation is much faster for the UFG Al 7.5 Mg alloy. Pit nucleation at early stages of exposure provides initiation sites for fatigue crack initiation, which ultimately result in an accelerated failure cycle, but the rate at which the crack grows may vary. It has been reported that higher crack growth rates in marine environments are accompanied by decreases in fatigue crack growth thresholds [80,82]. The primary mechanism inhibiting crack growth at higher stress ranges is corrosion induced crack closure [80,82]. This mechanism essentially inhibits crack growth through the expansion of corrosive products near the crack tip, inhibiting opening and closing at the crack face. Crack growth is more dependent on crack propagation mechanisms rather than initiation, providing a possible explanation as to why pitting has less of an effect on specimens tested at higher maximum stresses.

Increases in corrosion fatigue susceptibility for the UFG alloy at lower stress ranges are likely a result of the smooth fracture surface and lack of crack closure mechanisms synonymous with rough fracture surfaces; as explained by Pao et al. [82]. High degrees of surface roughness are thought to reduce the driving force near the crack tip, resulting in crack closure and increasing fatigue life [82]. Fine grain nanostructured materials lack this effect. The crack path of the UFG alloy was said to propagate in a straight line crack path, while the large grain alloys deviated to a zigzag pattern. It was concluded that high degrees of fracture surface roughness and deviation from straight crack paths result in lowered effective driving force at the crack tip [82]. It is believed a similar mechanism is active in the UFG Al–7.5 Mg alloys in this study.

4. Conclusions

The corrosion fatigue strength of a UFG Al–7.5 Mg alloy was investigated and compared to its conventional counterpart 5083 H111. The UFG Al–7.5 Mg alloy was observed to have superior fatigue limit than the conventional alloy in air. It was shown that under cyclic loading, the fatigue limit of the UFG alloy was drastically reduced when exposed to a marine environment. At high cyclic stresses the UFG alloy had a superior fatigue resistance compared to the conventional 5803 alloy. SEM analysis of the samples revealed that pitting corrosion on the sample surface acted as a stress concentrator in both alloys. Crack initiation sites resulting in fatigue failure were at second phase particles and inclusions. The experimental results suggest that at high stress ranges slip enhanced dissolution and hydrogen embrittlement were the dominant mechanisms for failure in the UFG Al–7.5 Mg alloy. Conversely, at lower applied maximum stress values, pitting was the prevailing mechanism which led to crack initiation and ultimate failure. Since pitting essentially relates to the lack of electrochemical stability of the protective film compared to the overall breakdown in a solution, it is inappropriate to relate pitting kinetics alone to low cycle fatigue. It is also believed that crack closure mechanisms are a factor in the fatigue performance of UFG alloys.

Acknowledgements

This work was sponsored by the Office of Naval Research (ONR) Grant #N00014-00-1-0153 and NACE International, seed Grant

#N000140210024. The authors would also like to thank The LaQue Testing and Research Center for their assistance in testing and analysis. The authors also wish to acknowledge Boeing Corporation and Enrique Lavernia at UC Irvine for providing the UFG (nano-structured) alloys.

References

[1] K.M. Youseff, R.O. Scattergodo, E.J. Murty, C.C. Koch, Nanocrystalline Al–Mg alloy with ultrahigh strength and good ductility, Scr. Mater. 54 (2006) 251–256.

[2] M.M. Sharma, C.W. Ziemian, Pitting and stress corrosion cracking susceptibility of nanostructured Al–Mg alloys in natural and artificial environments, J. Mater. Eng. Perform. 17 (2008) 870–878.

[3] J.C. Chang, T.H. Chuang, Stress-corrosion cracking susceptibility of the superplastically formed 5083 aluminum alloy in 3.5 pct NaCl solution, Metall. Mater. Trans. A 30A (1999) 3191–3199.

[4] R. Verma, A.K. Ghosh, S. Kim, C. Kim, Superplastic forming characteristics of fine-grained 5083 aluminum, J. Mater. Eng. Perform. 4 (5) (1995) 543–550.

[5] K.D. Ralston, N. Birbilis, Effect of grain size on corrosion: a review, Corrosion 66 (7) (2010) 0750051–07500513.

[6] G. Ben-Hamu, D. Eliezer, L. Wagner, The relation between severe plastic deformation microstructure and corrosion behavior of AZ31 magnesium alloy, J. Alloys Compd. 468 (1–2) (2009) 222–229.

[7] D. Song, A. Ma, J. Liang, P. Lin, D. Yang, J. Fan, Corrosion behavior of equal-channel-angular-pressed pure magnesium in NaCl aqueous solution, Corros. Sci. 52 (2010) 481–490.

[8] T. Zhang, Y. Shao, G. Meng, Z. Cui, F. Wang, Corrosion of hot extrusion AZ91 magnesium alloy: I-relation between the microstructure and corrosion behavior, Corros. Sci. 53 (2011) 1960–1968.

[9] D. Orlov, K.D. Ralston, N. Birbilis, Y. Estrin, Enhanced corrosion resistance of Mg alloy ZK60 after processing by integrated extrusion and equal channel angular pressing, Acta Mater. 59 (2011) 6176–6186.

[10] C. Op'tHoog, N. Birbilis, Y. Estrin, Corrosion of pure Mg as a function of grain size and processing route, Adv. Eng. Mater. 10 (2008) 579–582.

[11] N. Aung, W. Zhou, Effect of grain size and twins on corrosion behaviour of AZ31B magnesium alloy, Corros. Sci. 52 (2010) 589–594.

[12] T. Zhang, Z. Ji, S. Wu, Effect of extrusion ratio on mechanical and corrosion properties of AZ31B alloys prepared by a solid recycling process, Mater. Des. 32 (2011) 2742–2748.

[13] Jinsun Liao, Makoto Hotta, Shin-ichi Motoda, Tadashi Shinohara, Atmospheric corrosion of two field-exposed AZ31B magnesium alloys with different grain size, Corros. Sci. 71 (2013) 53–61.

[14] J. Liao, M. Hotta, N. Yamamoto, Corrosion behavior of fine-grained AZ31B magnesium alloy, Corros. Sci. 61 (2012) 208–214.

[15] M.M. Sharma, J.D. Tomedi, T.J. Weigley, Slow strain rate testing and stress corrosion cracking of ultra-fine grained and conventional Al–Mg alloy, Mater. Sci. Eng., A 619 (2014) 35–46.

[16] R.M. Pidaparti, R.R. Patel, Correlation between corrosion pits and stresses in Al alloys, Mater. Lett. 62 (2008) 4497–4499.

[17] P. Marcus, J. Oudar (Eds.), Corrosion Mechanisms in Theory and Practice, Marcel Dekker, New York, 1995.

[18] L.L. Shreie, R.A. Jarman, C.T. Burstein (Eds.), Corrosion—Metal/Environmental Reactions, third ed., Butterworth & Heinemann Ltd., Oxford, 1994.

[19] H.H. Strehblow, Mechanisms of pitting corrosion. Corrosion Mechanisms in Theory and Practice. Marcel Dekker, New York, 1995, pp. 201–238.

[20] G.T. Burstein, C. Liu, R.M. Souto, S.P. Vines, Origins of pitting corrosion, Corros. Eng., Sci. Technol. 39 (1) (2004) 25–30.

[21] R.P. Wei, C.M. Liao, M. Gao, A transmission electron microscopy study of 7075-T6 and 2024-T3 aluminum alloys, Metall. Mater. Trans. A 29A (1998) 1153–1160.

[22] S. Suresh, Fatigue of Materials, second ed., Cambridge University Press, Cambridge, 1998.

[23] R.W. Hayes, V.L. Tellkamp, E.J. Lavernia, Creep behavior of a cryomilled ultrafine-grained Al–4% Mg alloy, J. Mater. Res. 15 (10) (2000) 2215–2222.

[24] V.L. Tellkamp, E.J. Lavernia, Processing and mechanical properties of nanocrystalline 5083 Al alloy, Nanostruct. Mater. 12 (1999) 249–254.

[25] P.S. Pao, H.N. Jones, S.J. Gill, C.R. Feng, Tensile deformation and fatigue crack growth in bulk nanocrystalline Al–7.5 Mg, MRS Symp. Proc. Vol. 740 (2003) 15–20.

[26] E. Sikora, X.J. Wei, B.A. Shaw, Corrosion behavior of nanocrystalline bulk Al–Mg based alloys, Corrosion 60 (4) (2004) 387–397.

[27] A. Aballe, M. Bethencourt, F.J. Botana, M.J. Cano, M. Marcos, Corros. Sci. 43 (2001) 1657–1674.

[28] A. Aballe, M. Bethencourt, F.J. Botana, M. Marcos, J.M. Sanchez-Amaya, Influence of the degree of polishing of alloy AA 5083 on its behavior against localized alkaline corrosion, Corros. Sci. 46 (2004) 1909–1920.

[29] I.N.A. Oguocha, O.J. Adigun, S. Yannacopoulos, Effect of sensitization heat treatment on properties of Al–Mg alloy AA5083-H116, J. Mater. Sci. 43 (2008) 4208–4214.

[30] R.L. Holtz, P.S. Pao, R.A. Bayles, T.M. Longazel, R. Goswami, Corrosion–fatigue behavior of aluminum alloy 5083-H131 sensitized at 448 K (175 °C), Metall. Mater. Trans. A 43 (2012) 2839–2849.

[31] J.A. Lyndon, R.K. Gupta, M.A. Gibson, N. Birbilis, Electrochemical behaviour of the β-phase intermetallic (Mg_2Al_3) as a function of pH as relevant to corrosion of aluminium–magnesium alloys, Corros. Sci. 70 (2013) 290–293.

[32] Z. Zhong, N.P. Hung, Grinding of alumina/aluminum composites, J. Mater. Proc. Tech. 123 (2002) 13–17.

[33] T.I. Wu, Jian Kuo Wu, Effects of surface condition and metallurgical practice on the corrosion behaviour of AA 7075 aluminium alloy, Corros. Prev. Control 43 (1) (1996) 20–26.

[34] Marcos Lugoa, J.B. Jordonb, M.F. Horstemeyer, M.A. Tschoppa, J. Harris, A.M. Gokhale, Quantification of damage evolution in a 7075 aluminum alloy using an acoustic emission technique, Mater. Sci. Eng., A 528 (2011) 6708–6714.

[35] S.-M. Moon, S.-I. Pyun, Faradaic reactions and their effects on dissolution of the natural oxide film on pure aluminum during cathodic polarization in aqueous solutions, Corrosion 54 (7) (1998) 546–547.

[36] C.A. Walton, H.J. Martin, M.F. Horstemeyer, W.R. Whittington, C.J. Horstemeyer, P.T. Wang, Corrosion stress relaxation and tensile strength effects in an extruded AZ31 magnesium alloy, Corros. Sci. 80 (2014) 503–510.

[37] Weiwei Song, Holly J. Martin, Ayesha Hicks, Denver Seely, Christopher A. Walton, William B. Lawrimore II, Paul T. Wang, M.F. Horstemeyer, Corrosion behaviour of extruded AM30 magnesium alloy under salt-spray and immersion environments, Corros. Sci. 78 (2014) 353–368.

[38] P. Wittke, M. Klein, F. Walther, Corrosion fatigue behaviour of creep-resistant magnesium alloy Mg–4Al–2Ba–2Ca, Proc. Eng. 74 (2014) 78–83.

[39] M. Esmaily, M. Shahabi-Navid, J.-E. Svensson, M. Halvarsson, L. Nyborg, Y. Cao, L.-G. Johansson, Influence of temperature on the atmospheric corrosion of the Mg–Al alloy AM50, Corros. Sci. (2014) http://dx.doi.org/10.1016/j.corsci.2014.10.040.

[40] Mohsen Danaie, Robert Matthew Asmussen, Pellumb Jakupi, David W. Shoesmith, Gianluigi A. Botton, The role of aluminum distribution on the local corrosion resistance of the microstructure in a sand-cast AM50 alloy, Corros. Sci. 77 (2013) 151–163.

[41] G. Song, A. Atrens, Understanding magnesium corrosion – a framework for improved alloy performance, Adv. Eng. Mater. 5 (2003) 837–858.

[42] K. Spencer, M.X. Zhang, Heat treatment of cold spray coatings to form protective intermetallic layers, Scr. Mater. 61 (2009) 44–47.

[43] N. Birbilis, R.G. Buchheit, Electrochemical characteristics of intermetallic phases in aluminum alloys: an experimental survey and discussion, J. Electrochem. Soc. 152 (2005) B140–B151.

[44] E. Bumiller, R.G. Kelly, Intergranular corrosion in AA5XXX: a case for continuous attack with a discontinuous active path, 2011 DoD Corrosion Conference, Palm Springs, CA, NACE, 2011.

[45] G. Scamans, Low temperature sensitization of AA5xxx alloys, Technical Report IR07-197, Innoval, Oxon, UK, 2008.

[46] N. Birbilis, R. Zhang, M.L.C. Lim, R.K. Gupta, C.H.J. Davies, S.P. Lynch, R.G. Kelly, J.R. Scully, Quantification of sensitization in AA5083-H131 via imaging Ga embrittled fracture surfaces, Corrosion 69 (4) (2013) 396–402.

[47] R.K. Gupta, Y. Wang, R. Fang, N.L. Sukiman, C.H.J. Davies, N. Birbilis, Imparting sensitization resistance to an Al–5Mg alloy via neodymium additions, Corrosion 69 (1) (2013) 4–8.

[48] M.L.C. Lim, J.R. Scully, R.G. Kelly, Intergranular corrosion penetration in an Al–Mg alloy as a function of electrochemical and metallurgical conditions, Corrosion 69 (1) (2013) 35–47.

[49] M.C. Carroll, P.I. Gouma, M.J. Mills, G.S. Daehn, B.R. Dunbar, Effects of Zn additions on the grain boundary precipitation and corrosion of Al-5083, Scr. Mater. 42 (2000) 335–340.

[50] R. Jones, D. Baer, M. Danielson, J. Vetrano, Role of Mg in the stress corrosion cracking of an Al–Mg alloy, Metall. Mater. Trans. A 32 (2001) 1699–1711.

[51] J. Searles, P. Gouma, R. Buchheit, Stress corrosion cracking of sensitized AA5083 (Al–4.5Mg–1.0Mn), Metall. Mater. Trans. A 32 (2001) 2859–2867.

[52] Ming Liu, Patrik Schmutz, Sandrine Zanna, Antoine Seyeux, Helene Ardelean, Guangling Song, Andrej Atrens, Philippe Marcus, Electrochemical reactivity, surface composition and corrosion mechanisms of the complex metallic alloy Al_3Mg_2, Corros. Sci. 52 (2010) 562–578.

[53] B. Mazurkiewicz, The electrochemical behaviour of the Al_8Mg_5 intermetallic compound, Corros. Sci. 23 (1983) 687–696.

[54] D.R. Baer, J.C.F. Windisch, M.H. Engelhard, M.J. Danielson, R.H. Jones, J.S. Vetrano, Influence of Mg on the corrosion of Al, J. Vac. Sci. Technol., A 18 (1) (2000) 131–136.

[55] G. Palasantzas, D.T.L. van Agterveld, J.T.M. De Hosson, Electron beam induced oxidation of Al–Mg alloy surfaces, Appl. Surf. Sci. 191 (2002) 266–272.

[56] Ming Liu, Patrick Schmutz, A. Barnes, N.A. Senior, R.C. Newman, Film-induced cleavage of Ag–Au alloys, Metall. Mater. Trans. A – Phys. Metall. Mater. Sci. 40A (2009) 58–68.

[57] R.C. Newman, Stress corrosion cracking of noble metals and their alloys in solutions containing cations of the noble metal: review of observations relevant to competing models of SCC, Corros. Sci. 50 (2008) 1807–1810.

[58] J. Deakin, Z.H. Dong, B. Lynch, R.C. Newman, De-alloying of type 316 stainless steel in hot, concentrated sodium hydroxide solution, Corros. Sci. 46 (2004) 2117–2133.

[59] A. Barnes, R.C. Newman, Progress in testing the film-induced cleavage model of stress corrosion cracking, Met. Mater. Proc. 8 (1996) 211–217.

[60] T. Shahrabi, R.C. Newman, K. Sieradzki, Stress-corrosion cracking of alpha-brass without copper oxidation, J. Electrochem. Soc. 140 (1993) 348–352.

[61] M. Saito, G.S. Smith, R.C. Newman, Testing the film-induced cleavage model of stress-corrosion cracking, in: International Conference to Mark the 20th Anniversary of the UMIST Corrosion-and-Protection-Centre: Advances in

Corrosion and Protection, Pergamon-Elsevier Science Ltd., Manchester, United Kingdom, pp. 411–417.
[62] R.G. Kelly, A.J. Frost, T. Shahrabi, R.C. Newman, Brittle-fracture of an Au/Ag alloy induced by a surface-film, Metall. Mater. Trans. A – Phys. Metall. Mater. Sci. 22 (1991) 531–541.
[63] M. Liu, S. Zanna, H. Ardelean, I. Frateur, P. Schmutz, G. Song, A. Atrens, P. Marcus, A first quantitative XPS study of the surface films formed, by exposure to water, on Mg and on the Mg–Al intermetallics: Al_3Mg_2 and $Mg_{17}Al_{12}$, Corros. Sci. 51 (2009) 1115–1127.
[64] K.A. Yasakau, M.L. Zheludkevich, S.V. Lamaka, M.G.S. Ferreira, Role of phases in localized corrosion of AA5083, Electrochim. Acta 52 (2007) 7651–7659.
[65] Zhao, Z. Qi, X. Wang, Z. Zhang, Fabrication and characterization of monolithic nanoporous copper through chemical dealloying of Mg–Cu alloys, Corros. Sci. 51 (9) (2009) 2120–2125.
[66] B. Zberg, P.J. Uggowitzer, J.F. Loffler, MgZnCa glasses without clinically observable hydrogen evolution for biodegradable implants, Nat. Mater. 8 (2009) 887–891.
[67] R.H. Jones, Stress-corrosion cracking, in: A.I.H. Committee (Ed.), ASM Handbook, vol. 13A, ASM International, Ohio, 2010, pp. 346–366.
[68] T. Hanlon, Y.-N. Kwon, S. Suresh, Grain size effects on the fatigue response of nanocrystalline metals, Scr. Mater. 49 (2003) 675–680.
[69] P.S. Pao, H.N. Jones, S.F. Cheng, C.R. Feng, Fatigue crack propagation in ultrafine grained Al–Mg alloy, Int. J. Fatigue 27 (2005) 1164–1169.
[70] K. Sadananda, A.K. Vasudevan, Review of environmentally assisted cracking, Metall. Mater. Trans. A 42A (2011) 279–295.
[71] C. Laird, D.J. Duquette, in: O. Devereux, A.J. McEvily, R.W. Staehle (Eds.), Corrosion Fatigue: Chemistry, Mechanics and Microstructure, NACE Houston, TX, 1972, p. 88.
[72] D.J. Duquette, in: R. Gibala, R.F. Hehermann (Eds.), Hydrogen Embrittlement and Stress Corrosion Cracking, ASM, Metals Park, OH, 1984, p. 249.
[73] T.S. Srivatsan, T.S. Sudarshan, Mechanisms of fatigue crack initiation in metals: role of aqueous environments, J. Mater. Sci. 23 (1988) 1521–1533.
[74] G.S. Chen, D.J. Duquette, Corrosion fatigue of a precipitation-hardened Al–Li–Zr Alloy in a 0.5 M sodium chloride solution, Metall. Trans. A 23 (5) (1992) 1563–1572.
[75] C. Menzemer, T.S. Srivatsan, The effect of environment on fatigue crack growth behavior of aluminum alloy 5456, Mater. Sci. Eng., A 271 (1991) 188–195.
[76] R.H. Jones, V.Y. Gertsman, J.S. Vetrano, C.F. Windisch Jr., Crack-particle interactions during intergranular stress corrosion of AA5083 as observed by cross-section transmission electron microscopy, Scr. Mater. 50 (2004) 1355–1359.
[77] R.H. Jones, J.S. Vetrano, C.F. Windisch Jr., Stress corrosion cracking of Al–Mg and Mg–Al alloys, Corros. Sci. 60 (2004) 1144–1154.
[78] J. Farmer, S. Menon, General Corrosion, Localized Corrosion and Environmental Cracking of Modern Engineering Materials, Encyclopedia of Life Support Systems, EOLSS Publishers Company Limited, United Kingdom, 2011.
[79] H.A. Padilla II, B.L. Boyce, A review of fatigue behavior in nanocrystalline metals, Exp. Mech. 50 (2010) 5–23.
[80] Y. Yang, B.I. Imasogie, S.M. Allameh, B. Boyce, K. Lian, J. Lou, W.O. Soboyejo, Mechanisms of fatigue in LIGA Ni MEMS thin films, Mater. Sci. Eng., A 444 (2007) 39–50.
[81] B.L. Boyce, J.R. Michael, R.G. Kotula, Fatigue of metallic microdevices and the role of fatigue-induced surface oxides, Acta Mater. 52 (2004) 1609–1619.
[82] P.S. Pao, H.N. Jones, S.F. Cheng, C.R. Feng, Fatigue crack propagation in ultrafine grained Al–Mg alloy, Int. J. Fatigue 27 (2005) 1164–1169.